Lead-free organic inorganic halide perovskite solar cell with over 30% efficiency

Md. A. Islam[a,*] Md. N. Bin Alamgir[b], S. I. Chowdhury[b], S. M. B. Billah[b]
[a]*Department of Materials Science and Engineering, Rajshahi University of Engineering and Technology, Rajshahi, Bangladesh.*
[b]*Department of Electrical and Electronic Engineering, East Delta University, Abdullah Al Noman Road, Noman Society, East Nasirabad, Khulshi, Chattogram 4209, Bangladesh*

In this study, numerical analysis on an Sn-based planner heterojunction perovskite device structure of Glass/ FTO/ ZnO/ $CH_3NH_3SnI_3$/ CZTS/ Metal, with $CH_3NH_3SnI_3$ as an absorber layer, was performed by using the solar cell device simulator SCAPS 1D. As an electron transport layer (ETL) and a hole transport layer (HTL), inorganic materials ZnO and CZTS (kesterite) were used. To optimize the device, the thickness of the absorber, electron, and hole transport layers, defect density, and absorber doping concentrations were varied, and their impact on device performance was evaluated. The effect of temperature and work function of various anode materials were also investigated. The optimum absorber layer thickness was found at 750 nm for the proposed structure. The acceptor concentration with a reduced defect density of the absorber layer enhances device performance significantly. For better performance, a higher work function anode material is required. The optimized solar cell achieved a maximum power conversion efficiency of 30.41% with an open-circuit voltage of 1.03 V, a short circuit current density of 34.31 $mA/cm^{2,}$ and a Fill Factor 86.39%. The proposed cell structure also possesses an excellent performance under high operating temperature indicating great promise for eco-friendly, low-cost solar energy harvesting.

(Received February 5, 2022; Accepted May 25, 2022)

Keywords: Perovskite solar cell, Lead-free, SCAPS, High efficiency, Defect density, Temperature effect.

1. Introduction

Electrical energy demand increases day by day with the increase of industrialization and civilization, and most of the needs are full filed from the fossil fuels burning. Fossil fuel burning is one of the significant causes of global warming and severely pollutes the environment. So, the demand for clean and renewable energy sources increases progressively [1, 2]. Energy harvesting from solar radiation by photovoltaic technology has emerged as the most sustainable, clean, and eco-friendly renewable energy source to meet the world's energy demand [3]. Solar cell technology has developed throughout time due to decades of research by scientists. Perovskite is a 3rd generation solar cell and a potential candidate for dominating other photovoltaic technologies due to its easy and low-cost manufacturing technique [4]. It also possesses excellent optical and electrical properties such as ideal band gap, transport of ambipolar charge carriers, long charge diffusion lengths, high absorption coefficient, and low exciton bond energy [5-8]. Power conversion efficiency (PCE) of Perovskite Solar Cell (PSC) increases promptly and exceeded 25% recently [9, 10]. However, it was relatively low (3.8%) when researchers started working on it in 2009 [11] that makes it dominant in research interest in the global photovoltaic market. The general structure of perovskite material is ABX_3 (octahedral), where A, B are cations and X is the anion [12]. This structure makes it an excellent light absorber [13], and the photon energy can be converted into electricity using the photovoltaic effect [14]. The methylammonium (MA) lead halide is one of the promising perovskite absorber s with excellent photovoltaic performance [15]. Despite its superb properties and PCE, it faces significant problems in commercialization due to

* Corresponding author: aminulmse@gmail.com
https://doi.org/10.15251/JOR.2022.183.395

toxic Lead (Pb) and stability issues [16-19]. Researchers have proposed numerous Lead-free perovskites where Pb is substituted by Sn (II), Ge(II), Bi(III), Sb(III), Ti (IV), etc. [20]. Sn-based methylammonium halide ($MASnI_3$) has become most popular due to its outstanding optoelectronic features. $MASnI_3$ possesses a direct band gap of 1.3 eV that can extract a larger range of the spectrum compared to lead-based perovskite materials [21]. On the other hand, TiO_2 is a popular electron transport layer (ETL) for PSC. However, it requires high fabrication temperature which increases cost in manicuring of PSCs [22]. ZnO can be an alternative for TiO_2 because of its wide band gap, higher electron mobility, simpler and low-cost fabrication technique [22]. Recently, $Cu_2Zn_2Sn_2S_2$ (CZTS) has been introduced as a hole transport layer (HTL) in PSCs [23]. CZTS is composed of abundant and nontoxic material with an amazing electrical and optical properties. It is widely recognized in the solar industry for its direct band gap, high hole mobility, and high absorption coefficient [24]. Researchers are working on developing solar cells with high efficiency, low-cost, and eco-friendly. The device structure proposed in this study, is unique and highly efficient apart from all existing devices, making it a viable contender for future solar cell technology fulfilling the demands. Solar cell capacitance simulator (SCAPS) is used to optimize the different parameters such as layer thickness, doping concentration. The effect of defect density operating temperature and metalwork function on the proposed solar cell were also investigated.

2. Device structure and simulation methodology

2.1. Device structure

This work is a numerical simulation of a planer heterojunction Sn-based perovskite solar cell that performs under illumination AM 1.5G at 300K using SACPS-1D (3.3.08). Three main equations, i.e., the Poisson equation (1), electron continuity equation (2), and hole continuity equation (3), are used to simulate SCAPS-1D.

$$\frac{d}{dx}\left(-\varepsilon(x)\frac{d\psi}{dx}\right) = q[p(x) - n(x) + N_D^+(x) - N_A^-(x) + p_t(x) - n_t(x)] \quad (1)$$

$$\frac{dp_n}{dt} = G_p - \frac{p_n - p_{n0}}{\tau_p} + p_n\mu_p\frac{d\xi}{dx} + \mu_p\xi\frac{dp_n}{dx} + D_p\frac{d^2p_n}{dx^2} \quad (2)$$

$$\frac{dn_p}{dt} = G_p - \frac{n_p - p_{p0}}{\tau_n} + n_p\mu_n\frac{d\xi}{dx} + \mu_n\xi\frac{dn_p}{dx} + D_n\frac{d^2n_p}{dx^2} \quad (3)$$

where D, ξ, G, Ψ, q, τ_p, τ_n, μ_p, μ_n, $n_t(x)$, $n(x)$, $p_t(x)$, $p(x)$, $N_D^+(x)$ and $N_A^-(x)$ denote diffusion coefficient, electric field, generation rate, electrostatic potential, electron charge, hole lifetime, electron lifetime, hole mobility, electron mobility, trapped electrons concentration, free electrons concentration, trapped holes concentration, free holes concentration, the concentration of ionized donor, and concentration of ionized acceptor respectively. The direction along the thickness is denoted by x [25]. Seven different layers of heterostructure solar cells can be designed in SCAPS-1D, and both light and dark environments can be simulated [26, 27]. The simulated solar cell device configuration was FTO/ZnO/$MASnI_3$ (Light absorbing layer)/CZTS/Pt. The band diagram and grading of energy parameter are shown in Figure 1 (a-c), where p-type CZTS was used as a hole transport layer, $MASnI_3$ as an absorber layer, and n-type ZnO as an electron transport layer. Furthermore, SnO_2: F (FTO) was used as the transparent contact material, and various materials such as Cu, Ag, Au, Cr, Ni, and Pt were used as anodes. Band alignment of energy levels is very crucial in terms of solar cell device functionality. The valence band and conduction band alignment for each of the layers used in this investigation is shown in Figure 1(b,c), beginning with the ETL and progressing to the Perovskite and HTL layers.

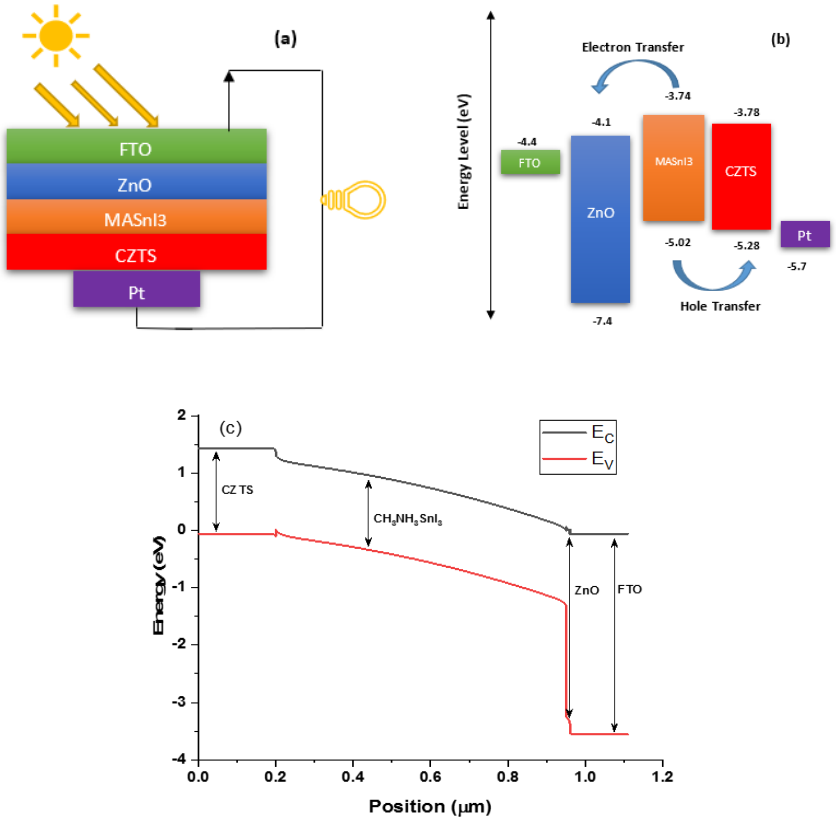

Fig. 1. (a) Simulated PSC device configuration, (b) Energy band diagram, and (c) grading of energy parameters of the device.

2.2. SCAPS simulation methodology

The device parameter values were selected from experiments, literature, and theories. The primary physical parameters used in the simulation are listed in Table 1, and Table 2 shows the defect parameters within the absorber layer and at the device layer interfaces.

Table 1. The basic parameters of each PSC layers [1, 4, 24, 28, 29].

Parameters	**FTO (TCO)**	**ZnO (ETL)**	**$CH_3NH_3SnI_3$ (absorber)**	**CZTS (HTL)**
Thickness (nm)	100	10 (variable)	750 (variable)	200 (variable)
Bandgap energy, E_g (eV)	3.4	3.33	1.3	1.49
Electron affinity, χ (eV)	4.5	4.1	4.17	4.1
Relative permittivity, ε_r	9.1	9.0	8.2	7
Conduction band density of states, N_c (cm^{-3})	1.1×10^{19}	2.2×10^{18}	1×10^{18}	2.2×10^{18}
Valance band density of states, N_v (cm^{-3})	1.1×10^{19}	1.9×10^{19}	1×10^{18}	1.8×10^{19}
Thermal velocity of electron and hole, (cm/s)	1×10^{7}	1×10^{7}	1×10^{7}	1×10^{7}
Electron mobility, μ_n (cm^2/Vs)	20	100	1.6	25
Hole mobility, μ_p (cm^2/Vs)	10	25	1.6	20
Donor concentration, N_D (cm^{-3})	1.1×10^{19}	1×10^{18}	0	0
Acceptor concentration, N_A (cm^{-3})	0	0	1×10^{16} (variable)	1.7×10^{18}

Table 2. Defect parameters of absorber layer and device at interfaces [1, 4, 21, 24, 28, 29].

Parameters	**ZnO**	**$CH_3NH_3SnI_3$**	**CZTS**	**ZnO /$CH_3NH_3SnI_3$ interface**	**$CH_3NH_3SnI_3$/ CZTS interface**
Defect type	Neutral	Neutral	Neutral	Neutral	Neutral
σ_n (cm^{-2})	1×10^{-15}	1×10^{-15}	1×10^{-15}	1×10^{-15}	1×10^{-15}
σ_p (cm^{-2})	1×10^{-15}	1×10^{-15}	1×10^{-15}	1×10^{-15}	1×10^{-15}
Energy distribution	Single	Gaussian	Single	Single	Single
Characteristic energy (eV)	–	0.100	–	–	–
Energy level with respect to E_v (above E_v) (eV)	0.600	0.600	0.100	0.600	0.600
Defect density, N_t (cm^{-3})	1×10^{15}	1×10^{15} (variable)	1×10^{15}	1×10^{10}	1×10^{10}

3. Result and discussion

3.1. Optimization of thickness

The absorber layer significantly influences the device's performance. The thickness of the absorber layer affects photovoltaic characteristics such as J_{SC}, V_{OC}, FF, and PCE, according to a previously published paper [30, 31]. To investigate the effect of the thickness of absorber layer, width of the layer was varied from 100 nm to 1000 nm in the device simulation, while the other parameters in Tables 1 and 2 remained constant. Figure 2 shows the simulation results for the change of thickness of the absorber layer.

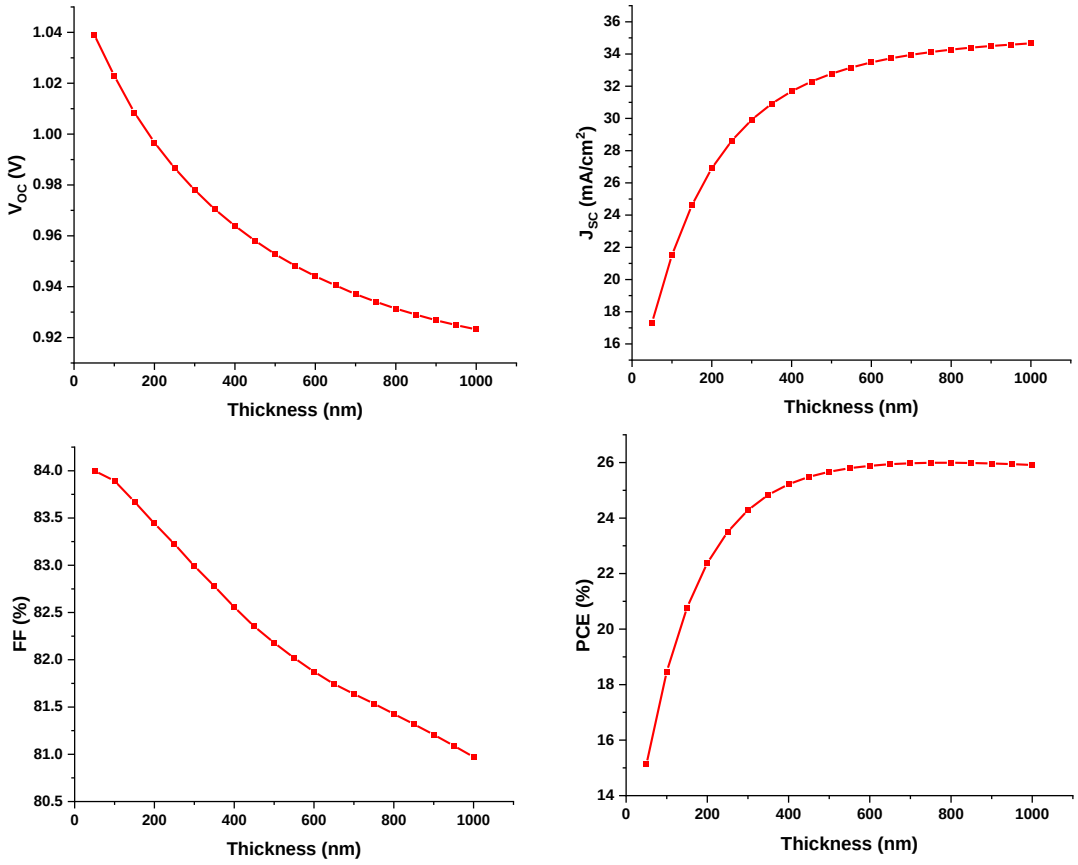

Fig. 2. Photovoltaic output as a function of absorber layer thickness.

The absorber layer thickness increases from 100 nm to 650 nm J_{SC} and PCE increased rapidly and become almost saturated at 750 nm. At 750 nm, J_{SC} was 34.1258 mA/cm^2 and the maximum J_{SC} (34.662 mA/cm^2) was obtained at 1000 nm because of the significant absorption coefficient of perovskite [25]. At the same time, V_{OC} and FF were decreased gradually with increasing the absorber layer thickness. V_{OC} decreases because of the enhancement of the recombination rate of free charge carriers with increasing the absorber layer thickness [30]. Increased series resistance could be the cause of reduction in Fill Factor as a function of absorber thickness [25, 32]. Initially, The PCE rises gradually with increase of absorbing layer's thickness and reached to maximum value of 25.99% at 750 nm and decreases with further increase of absorber thickness because of high recombination rate in thick absorber layers [25, 30, 33]. Effect of thickness of the electron and hole transport layers has been shown in Figure 3 and Figure 4 respectively. Changing the thickness of the ETL and HTL has a negligible effect on the device performance. The thicknesses of the ETL and HTL were increased from 10 nm to 100 nm. All parameters such as $V_{OC,}$ J_{SC} and efficiency become saturated after 20nm thickness of the ETL layer.

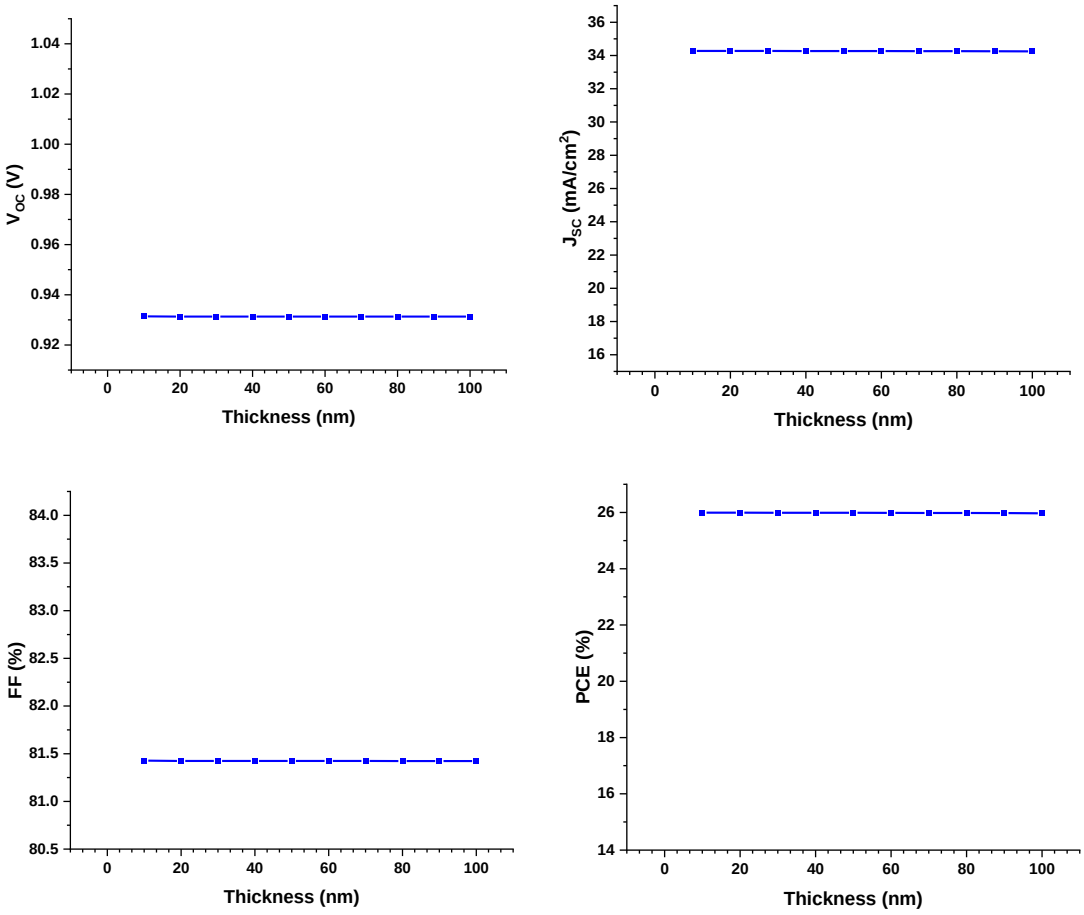

Fig. 3. Photovoltaic output as a function of ETL thickness.

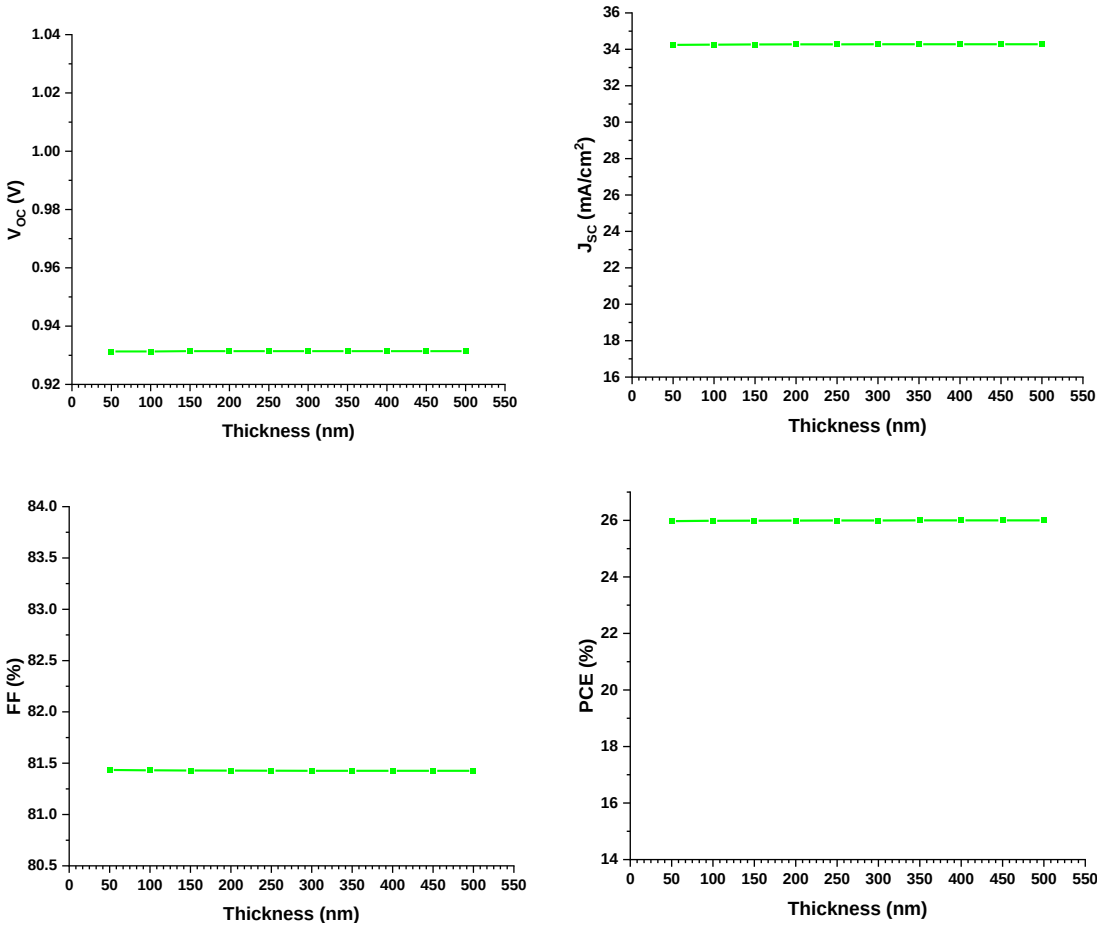

Fig. 4. Photovoltaic output as a function of HTL thickness.

3.2. Effect of acceptor doping density in the absorber layer

The acceptor doping density has a significant effect on the performance of perovskite solar cells. When $CH_3NH_3SnI_3$ expose to air because of oxidation, Sn^{2+} is converted into Sn^{4+}. So, it acts as a p-type semiconductor that affects the device's performance [34]. To avoid the formation of Sn^{2+} to Sn^{4+} SnO_2 is added to the $CH_3NH_3SnI_3$ [35, 36]. To find out the effect of acceptor carrier density in the absorber layer, the acceptor density is varied from 10^{14} to 10^{19} cm^{-3} as Takashi et al. reported that the acceptor density can be varied up to 10^{19} cm^{-3} [37]. Figure 5 shows the variation in different photovoltaic parameters with changing the acceptor doping density. A slight change in photovoltaic response up to 10^{16} cm^{-3} was observed. That means no significant differences was occurred in the generation of photo generated carriers with changing the acceptor density. Under the same photon energy incident, the total output of photo generated carriers remains constant regardless of acceptor density [33]. The Fermi energy level of the hole drops as the acceptor doping concentration increases, and consequently, V_{OC} rises, as shown in Figure 5. On other hand, J_{sc} first reduces moderately until 10^{16} cm^{-3} doping level after which it reduces rapidly. An increase in charge carrier recombination within the perovskite absorber layer could be the cause of decreasing J_{sc} [33]. The optimum acceptor concentration is adjusted at 10^{16} $cm^{-3,}$ and a maximum PCE of 26.91% was obtained for that concentration.

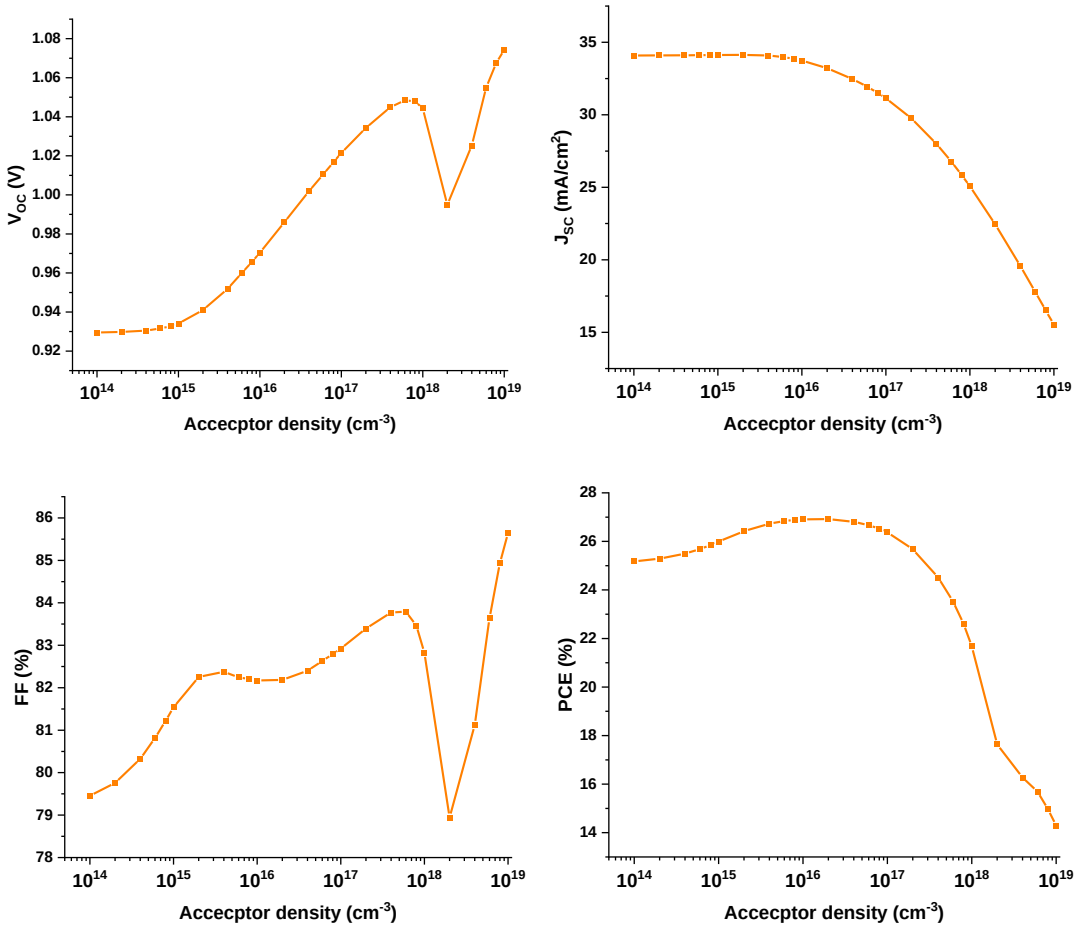

Fig. 5. Photovoltaic output as a function of acceptor concentration.

3.3. Effect of defect density in the absorber layer

Defect density is very crucial parameter to modify and control the performances of solar cell. The degradation phenomena such as PID of PV solar cell also depend on the defect density [38]. Various types of defects be existent within the perovskite absorber layer for example: lattice vacancies, interstitial, Schottky, and Frenkel defects as point defects. Aside from that, higher-order defects such as grain boundaries and dislocations also exist in the absorber layer [39]. Impurity defects in the absorber layer are produced during the self-doping process that converts the semiconductor to p-type [36, 40]. These defects introduce energy band gaps with shallow or deep levels. Charge carriers are trapped and boosted non radiative recombination result as a consequence of these defects [33, 39]. To investigate the influence of length of diffusion on photovoltaic responses, the electron's diffusion length was adjusted from 46 nm to 4600 nm while the defect density was varied from 10^{18} to 10^{14} cm^{-3}[41]. Hao et al. [40] Lazemi et al. [30] and Du et al. [33] have all used a similar method to modify defect density. The effect of defect densities on the photovoltaic characteristics is illustrated in Figure 6. It indicates that when the defect density increases, the device's performance reduces. The PCE was reduced to a low value of 6.12% at high defect density of 10^{18} cm^{-3} and the PCE was high (30.34%) at lower defect density of 10^{14} cm^{-3}. At lower defect density the device performance was enhanced significantly and approached to the SQ limit. At 10^{14} cm^{-3} defect level, the cell performances $J_{SC,}$ $V_{OC,}$ FF and PCE were 34.17 mA/cm^2, 1.03 V, 86.44%, and 30.37% respectively. The defect density influences the recombination rate specially the Shockley Read Hall (SRH) recombination category [25, 30, 42]. The recombination rate (R) can be mathematically expressed using the SRH model as equation (4). With increase of density defect, the recombination rate increases and charge carrier relaxation time decreases which results a low cell performance. Equation (5) expresses the lifetime of charge carriers ($\tau_{n,p}$). Positive

conduction band offset reduces the recombination between the absorber/buffer interfaces. According to Minemoto et al. [41], a CBO offset of around 0.3 eV reduces the recombination at the interface, optimizing the device performance [33]. Various researchers observe extensive carrier mobility, which indicates the large diffusion length [36, 42]. Equation (6) defines the diffusion length (L_D) of charge carriers.

$$R = \frac{\tau_{n,p}^{-1}(np - n_i^2)}{n + p + 2n_i coh(\frac{E_t - E_i}{kT})} \tag{4}$$

$$\tau_{n,p} = \frac{1}{\sigma_{n,p} v_{th} N_t} \tag{5}$$

$$L_D = \sqrt{D\tau} \tag{6}$$

where, E_t, E_i, v_{th}, n_i, n, p, $\sigma_{n,p}$, N_t, and D are the energy level of the trap defects, intrinsic energy level, charge carriers velocity, intrinsic density, electron density, hole density, capture cross section of charge carriers, defect density absorber layer and the diffusion coefficient, respectively.

3.4. Metal work function

The rectifying or ohmic behavior at the metal back contact/HTL interface was investigated by using various anode materials with different metal work functions. In this simulation, we have used Cr, Ag, Cu, Au, Ni, and Pt with work function of 4.5eV, 4.74 eV, 5.0 eV, 5.1 eV, 5.15eV and 5.7 eV, respectively [43, 44]. The barrier for the hole rises when the work function of contact materials decreases, as shown in Figure 7. Equation 7 expresses the potential energy barrier of surface (ϕ_B) at the anode/CZTS junctions.

$$\phi_B = \frac{E_g}{q} + \chi - \phi_M \tag{7}$$

where, E_g, χ, and ϕ_M are the bandgap of CZTS, the electron affinity of CZTS, and anode's work function, respectively.

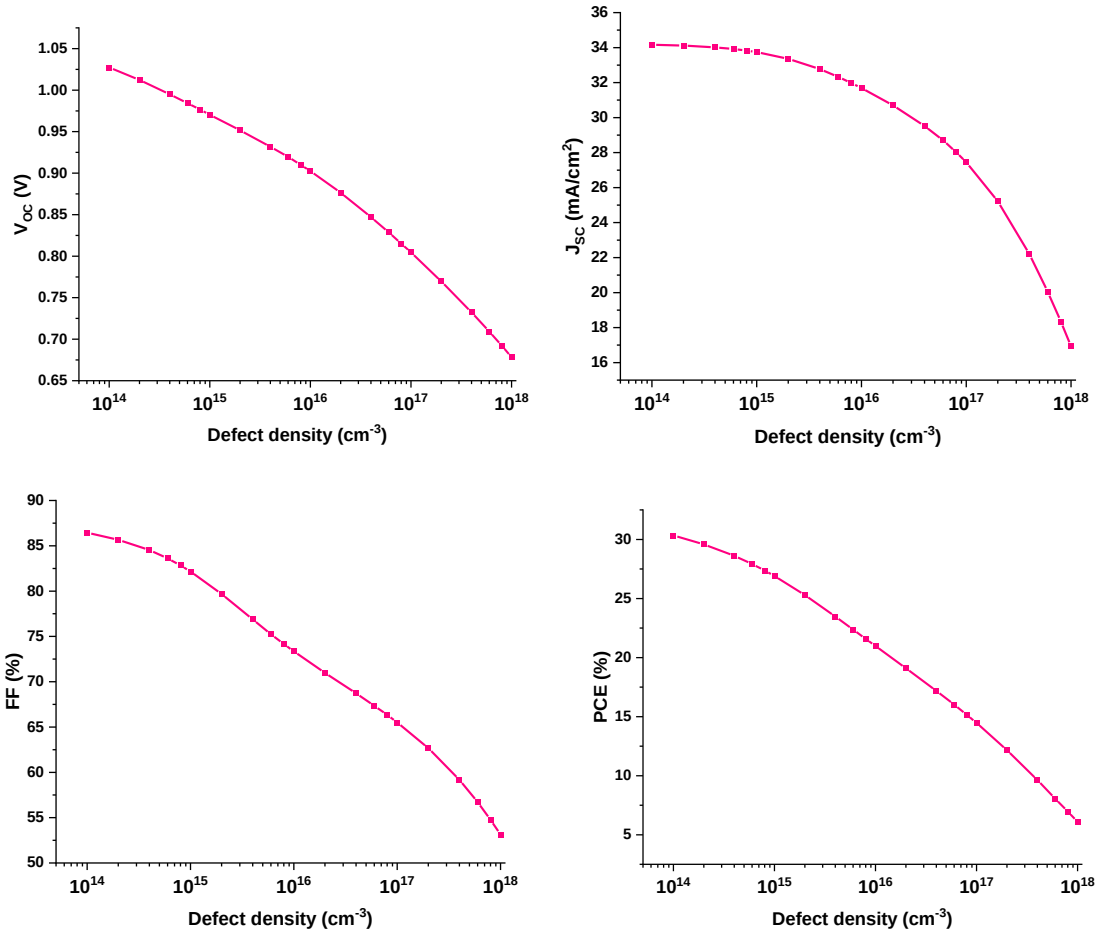

Fig. 6. Photovoltaic output as a function of defect density.

As the value of the metal work function increases, the energy barrier decreases, as expresses in Eq. 7, consequently the efficiency of the cell increases as shown in Figure 8.b. The impact of anode material on photovoltaic properties of PSC and J-V characteristics are depicted in Figure 8 (a, c). The PCE of the cell enhanced as the anode's metal work function increases.

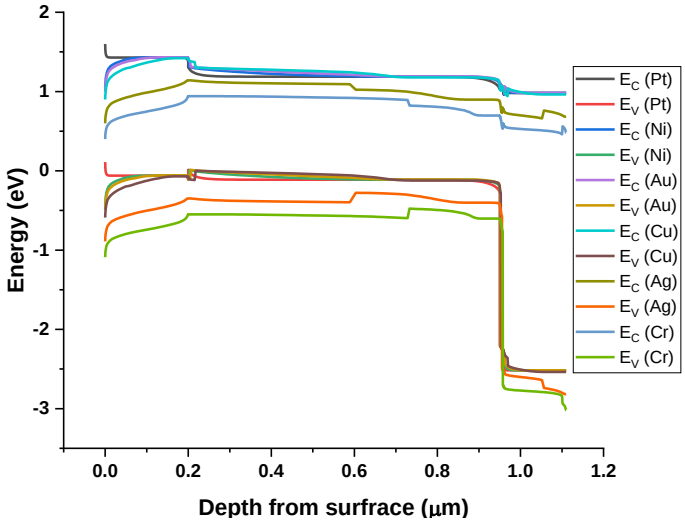

Fig. 7. PSC band diagram with different anode materials.

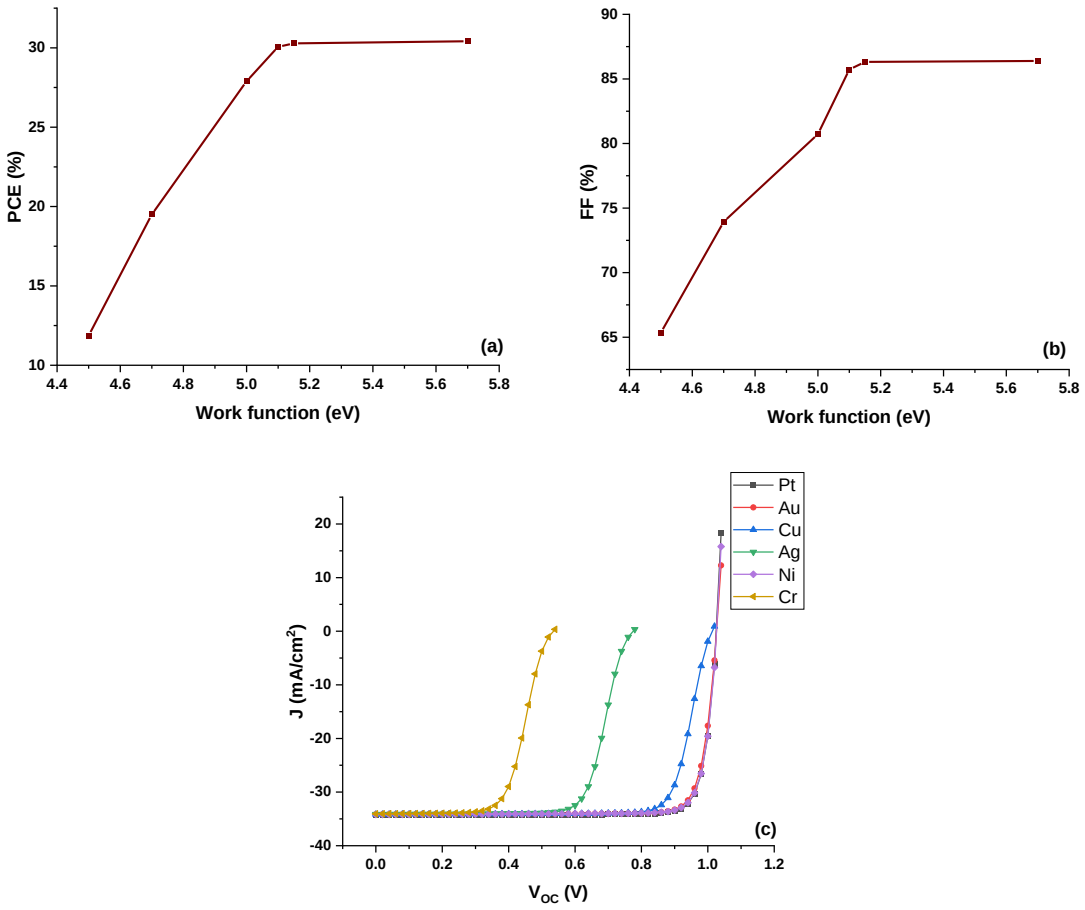

Fig. 8. (a) PCE and (b) FF of different anode material (c) Effect of work function on J-V characteristics.

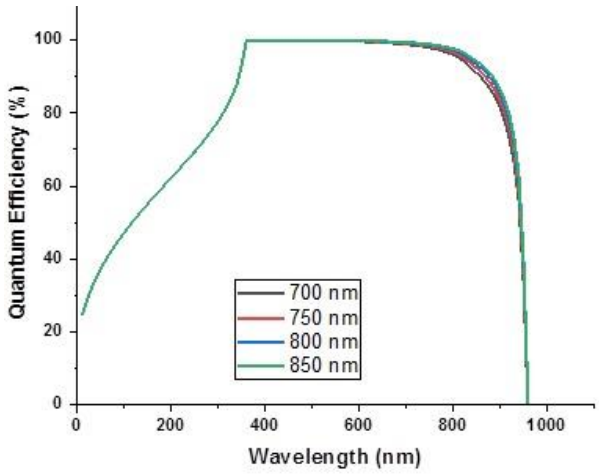

Fig. 9. Quantum efficiency curves with different thicknesses of the absorber layer.

Table 3. Comparison among some existing work.

Device Structure	Open Circuit Voltage (V)	Short Circuit Current (mA/cm^2)	Fill Factor (%)	Efficiency (%)	Reference
FTO/TiO2/ $CH_3NH_3SnI_3/CuO_2$/Pt	0.93	40.14	75.78	28.39	[1]
FTO/ZnO/$CH_3NH_3GeI_3$/$FAMASnGeI_3$/Cu_2O/Au	1.07	28.36	84.46	26.72	[2]
FTO/TiO_2/$FASnI_3$/Spiro-OMeTAD/Au	1.81	31.20	33.72	19.08	[20]
ZnO(nr)/ $CH_3NH_3SnI_3$/spiro-OMeTAD	0.9024	31.84	72.71	20.21	[45]
ZnO(nr)/ $CH_3NH_3SnI_3/Cu_2O$	0.8467	32.26	74.02	20.23	[45]
$Cd_{0.5}Zn_{0.5}S$/ $CH_3NH_3SnI_3$/$MASnBr_3$	0.96	32.48	76.40	23.86	[46]
In_2S_3/ $CH_3NH_3SnI_3$/Spiro-OMeTAD	0.75	33.44	77.28	19.32	[47]
FTO/ZnO/ $CH_3NH_3SnI_3$/CZTS/Pt	1.03	34.32	86.39	30.42	This work

3.5. Effect of operating temperature

The performances of the solar cell typical tested at STC condition having operating temperature of 25°C, however, in outdoor exposed condition, the cell temperature is reached to 60-65°C. To investigate the device's thermal performances, the cell temperature was varied from 283K to 373K in this simulation. The effect of temperature variation in Figure 10. With raise of temperature, the V_{OC} decreases significantly and the J_{SC} increases slightly. The decrease in V_{OC} with increasing temperature is caused by an increase in reverse saturation current [48]. Equation 8 governs the effect of temperature on V_{OC}.

$$V_{OC} = \frac{KT}{q}\ln\left(\frac{J_{SC}}{J_0} + 1\right) \quad (8)$$

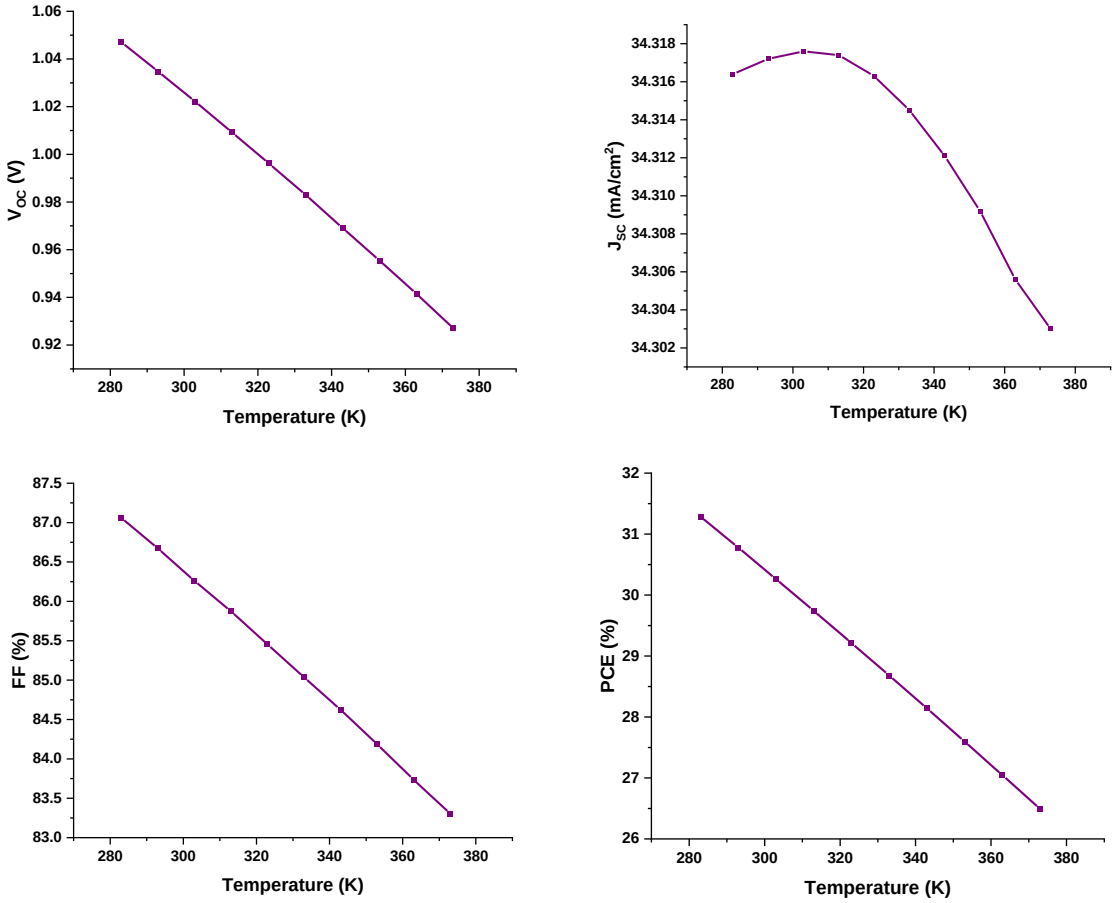

Fig. 10. Effect of the temperature on device performance with increasing temperature.

Here, J_0, K, T are the reverse saturation current, Boltzmann constant, and temperature, respectively. A slight increment in J_{SC} has been noted up to 313K, then drops. Increasing the temperature decreases the band gap of the absorber layer, requiring less energy for electrons to move from the valance band to the conduction band [48]. Furthermore, the change in J_{SC} is relatively tiny, and it is insufficient to affect the device performance at higher temperatures. Due to the dependence on V_{OC} and J_{SC}, efficiency and FF are high at low temperatures. At 283K, the device efficiency and FF were 31.29% and 87.06%, respectively. And it starts to decrease correspondingly as the temperature goes up.

4. Conclusion

In this simulation work, Glass/FTO/ZnO/$CH_3NH_3SnI_3$/CZTS/Pt, a planner heterojunction perovskite solar cell, was numerically analyzed by using solar cell device simulator SCAPS 1D. The effects of varying the thickness, defect density, and acceptor concentration of the perovskite layer, the work function of anode materials, and the impact of temperature variation on the performance of the proposed solar cell structure have been investigated. The optimal absorber thickness was 750 nm, and the lowered defect density of 10^{14} cm^{-3} in perovskite absorber layer significantly enhanced the photovoltaic performance and approached towards the SQ limit.

The significant concerns for future research are reducing defect density and enhancing Sn^{2+} stability of absorber layers, which might be addressed by upgrading the device's fabrication technology. An acceptor concentration of 10^{16} cm^{-3} of $CH_3NH_3SnI_3$ is adequate to attain desirable device performance. For lower work function materials, the Schottky barrier was developed at the anode/CZTS interface; thus, high work function materials, such as Pt, are required for ohmic contact. The obtained PCE, $V_{OC,}$ J_{SC} and FF were 30.42%, 1.03 V, 34.32 mA/cm^2, and 86.39% respectively with a broad-spectrum absorption (10-950nm) under optimal conditions. The simulation results achieved in this work would pave the way for an eco-friendly, low-cost, and high-efficiency PSC fabrication process.

References

[1] P. K. Patel, "Device simulation of highly efficient eco-friendly CH3NH3SnI3 perovskite solar cell," Scientific Reports, vol. 11, no. 1, pp. 1-11, 2021; https://doi.org/10.1038/s41598-021-82817-w

[2] N. Singh, A. Agarwal, and M. Agarwal, "Numerical simulation of highly efficient lead-free all-perovskite tandem solar cell," Solar Energy, vol. 208, pp. 399-410, 2020/09/15/ 2020; https://doi.org/10.1016/j.solener.2020.08.003

[3] D. J. Lipomi and Z. Bao, "Stretchable, elastic materials and devices for solar energy conversion," Energy & Environmental Science, 10.1039/C1EE01881G vol. 4, no. 9, pp. 3314-3328, 2011; https://doi.org/10.1039/c1ee01881g

[4] S. Ahmed, F. Jannat, M. A. K. Khan, and M. A. Alim, "Numerical development of eco-friendly Cs2TiBr6 based perovskite solar cell with all-inorganic charge transport materials via SCAPS-1D," Optik, vol. 225, p. 165765, 2021/01/01/ 2021; https://doi.org/10.1016/j.ijleo.2020.165765

[5] V. D'Innocenzo, G. Grancini, M. J. P. Alcocer, A. R. S. Kandada, S. D. Stranks, M. M. Lee, G. Lanzani, H. J. Snaith, and A. Petrozza, "Excitons versus free charges in organo-lead tri-halide perovskites," Nature Communications, vol. 5, no. 1, p. 3586, 2014/04/08 2014; https://doi.org/10.1038/ncomms4586

[6] S. D. Stranks, G. E. Eperon, G. Grancini, C. Menelaou, M. J. P. Alcocer, T. Leijtens, L. M. Herz, A. Petrozza, and H. J. Snaith, "Electron-Hole Diffusion Lengths Exceeding 1 Micrometer in an Organometal Trihalide Perovskite Absorber," Science, vol. 342, no. 6156, pp. 341-344, 2013; https://doi.org/10.1126/science.1243982

[7] J. S. Manser and P. V. Kamat, "Band filling with free charge carriers in organometal halide perovskites," Nature Photonics, vol. 8, no. 9, pp. 737-743, 2014/09/01 2014;

https://doi.org/10.1038/nphoton.2014.171

[8] T. Baikie, Y. Fang, J. M. Kadro, M. Schreyer, F. Wei, S. G. Mhaisalkar, M. Graetzel, and T. J. White, "Synthesis and crystal chemistry of the hybrid perovskite (CH3NH3)PbI3 for solid-state sensitised solar cell applications," Journal of Materials Chemistry A, 10.1039/C3TA10518K vol. 1, no. 18, pp. 5628-5641, 2013; https://doi.org/10.1039/c3ta10518k

[9] H.-S. Kim, S. H. Im, and N.-G. Park, "Organolead Halide Perovskite: New Horizons in Solar Cell Research," The Journal of Physical Chemistry C, vol. 118, no. 11, pp. 5615-5625, 2014/03/20 2014; https://doi.org/10.1021/jp409025w

[10] F. Gao, C. Li, L. Qin, L. Zhu, X. Huang, H. Liu, L. Liang, Y. Hou, Z. Lou, Y. Hu, and F. Teng, "Enhanced performance of tin halide perovskite solar cell by addition of lead thiocyanate," RSC Advances, 10.1039/C8RA00809D vol. 8, no. 25, pp. 14025-14030, 2018; https://doi.org/10.1039/C8RA00809D

[11] A. Kojima, K. Teshima, Y. Shirai, and T. Miyasaka, "Organometal Halide Perovskites as Visible-Light Sensitizers for Photovoltaic Cells," Journal of the American Chemical Society, vol. 131, no. 17, pp. 6050-6051, 2009/05/06 2009; https://doi.org/10.1021/ja809598r

[12] M. S. Chowdhury, S. A. Shahahmadi, P. Chelvanathan, S. K. Tiong, N. Amin, K. Techato, N. Nuthammachot, T. Chowdhury, and M. Suklueng, "Effect of deep-level defect density of the absorber layer and n/i interface in perovskite solar cells by SCAPS-1D," Results in Physics, vol. 16, p. 102839, 2020/03/01/ 2020; https://doi.org/10.1016/j.rinp.2019.102839

[13] T. Bendib, H. Bencherif, M. A. Abdi, F. Meddour, L. Dehimi, and M. Chahdi, "Combined optical-electrical modeling of perovskite solar cell with an optimized design," Optical Materials, vol. 109, p. 110259, 2020; https://doi.org/10.1016/j.optmat.2020.110259

[14] C. Mortan, T. Hellmann, M. Buchhorn, M. d'Eril Melzi, O. Clemens, T. Mayer, and W. Jaegermann, "Preparation of methylammonium lead iodide (CH3NH3PbI3) thin film perovskite solar cells by chemical vapor deposition using methylamine gas (CH3NH2) and hydrogen iodide gas," Energy Science Engineering, vol. 8, no. 9, pp. 3165-3173, 2020; https://doi.org/10.1002/ese3.734

[15] J. Burschka, N. Pellet, S.-J. Moon, R. Humphry-Baker, P. Gao, M. K. Nazeeruddin, and M. Grätzel, "Sequential deposition as a route to high-performance perovskite-sensitized solar cells," Nature, vol. 499, no. 7458, pp. 316-319, 2013/07/01 2013; https://doi.org/10.1038/nature12340

[16] F. Sani, S. Shafie, H. N. Lim, and A. O. Musa, "Advancement on Lead-Free Organic-Inorganic Halide Perovskite Solar Cells: A Review," (in eng), Materials (Basel), vol. 11, no. 6, p. 1008, 2018; https://doi.org/10.3390/ma11061008

[17] M. Caputo, N. Cefarin, A. Radivo, N. Demitri, L. Gigli, J. R. Plaisier, M. Panighel, G. Di Santo, S. Moretti, A. Giglia, M. Polentarutti, F. De Angelis, E. Mosconi, P. Umari, M. Tormen, and A. Goldoni, "Electronic structure of MAPbI3 and MAPbCl3: importance of band alignment," Scientific Reports, vol. 9, no. 1, p. 15159, 2019/10/22 2019; https://doi.org/10.1038/s41598-019-50108-0

[18] N. Guo, T. Zhang, G. Li, F. Xu, X. Qian, and Y. Zhao, "A simple fabrication of CH3NH3PbI3 perovskite for solar cells using low-purity PbI2," Journal of Semiconductors, vol. 38, no. 1, p. 014004, 2017; https://doi.org/10.1088/1674-4926/38/1/014004

[19] D. Liu, Q. Li, J. Hu, H. Jing, and K. Wu, "Predicted photovoltaic performance of lead-based hybrid perovskites under the influence of a mixed-cation approach: theoretical insights," Journal of Materials Chemistry C, 10.1039/C8TC04065F vol. 7, no. 2, pp. 371-379, 2019; https://doi.org/10.1039/C8TC04065F

[20] M. Kumar, A. Raj, A. Kumar, and A. Anshul, "An optimized lead-free formamidinium Sn-based perovskite solar cell design for high power conversion efficiency by SCAPS simulation," Optical Materials, vol. 108, p. 110213, 2020/10/01/ 2020; https://doi.org/10.1016/j.optmat.2020.110213

[21] D. Bartesaghi, A. H. Slavney, M. C. Gélvez-Rueda, B. A. Connor, F. C. Grozema, H. I. Karunadasa, and T. J. Savenije, "Charge Carrier Dynamics in Cs2AgBiBr6 Double Perovskite," The Journal of Physical Chemistry C, vol. 122, no. 9, pp. 4809-4816, 2018/03/08 2018; https://doi.org/10.1021/acs.jpcc.8b00572

[22] M. Dehghan and A. Behjat, "Deposition of zinc oxide as an electron transport layer in planar perovskite solar cells by spray and SILAR methods comparable with spin coating," RSC Advances, 10.1039/C9RA01839E vol. 9, no. 36, pp. 20917-20924, 2019; https://doi.org/10.1039/C9RA01839E

[23] H. T. Ali, M. Jamil, K. Mahmood, M. Yusuf, S. Ikram, A. Ali, N. Amin, K. Javaid, M. Y. Ali, and M. R. Nawaz, "A simulation study of perovskite based solar cells using CZTS as HTM with different electron transporting materials," Journal of Ovonic Research, vol. 17, no. 5, 2021.

[24] I. Kabir and S. A. Mahmood, "Comparative Study on Perovskite Solar Cells Using Inorganic Transport Layers," in 2019 IEEE International Conference on Telecommunications and Photonics (ICTP), 2019, pp. 1-4; https://doi.org/10.1109/ICTP48844.2019.9041784

[25] L. Lin, L. Jiang, P. Li, B. Fan, and Y. Qiu, "A modeled perovskite solar cell structure with a Cu2O hole-transporting layer enabling over 20% efficiency by low-cost low-temperature processing," Journal of Physics and Chemistry of Solids, vol. 124, pp. 205-211, 2019/01/01/ 2019; https://doi.org/10.1016/j.jpcs.2018.09.024

[26] S. Abdelaziz, A. Zekry, A. Shaker, and M. Abouelatta, "Investigating the performance of formamidinium tin-based perovskite solar cell by SCAPS device simulation," Optical Materials, vol. 101, p. 109738, 2020/03/01/ 2020; https://doi.org/10.1016/j.optmat.2020.109738

[27] M. Burgelman, P. Nollet, and S. Degrave, "Modelling polycrystalline semiconductor solar cells," Thin Solid Films, vol. 361-362, pp. 527-532, 2000/02/21/ 2000; https://doi.org/10.1016/S0040-6090(99)00825-1

[28] Gagandeep, M. Singh, and R. Kumar, "Simulation of perovskite solar cell with graphene as hole transporting material," in AIP Conference Proceedings, 2019, vol. 2115, no. 1, p. 030548: AIP Publishing LLC; https://doi.org/10.1063/1.5113387

[29] F. Baig, "Numerical analysis for efficiency enhancement of thin film solar cells," Universitat Politècnica de València, 2019.

[30] M. Lazemi, S. Asgharizadeh, and S. Bellucci, "A computational approach to interface engineering of lead-free CH3NH3SnI3 highly-efficient perovskite solar cells," Physical Chemistry Chemical Physics, 10.1039/C8CP03660H vol. 20, no. 40, pp. 25683-25692, 2018; https://doi.org/10.1039/C8CP03660H

[31] M. Liu, M. B. Johnston, and H. J. Snaith, "Efficient planar heterojunction perovskite solar cells by vapour deposition," Nature, vol. 501, no. 7467, pp. 395-398, 2013/09/01 2013; https://doi.org/10.1038/nature12509

[32] D.-Y. Son, J.-H. Im, H.-S. Kim, and N.-G. Park, "11% Efficient Perovskite Solar Cell Based on ZnO Nanorods: An Effective Charge Collection System," The Journal of Physical Chemistry C, vol. 118, no. 30, pp. 16567-16573, 2014/07/31 2014; https://doi.org/10.1021/jp412407j

[33] H.-J. Du, W.-C. Wang, and J.-Z. Zhu, "Device simulation of lead-free CH3NH3SnI3 perovskite solar cells with high efficiency," Chinese Physics B, vol. 25, no. 10, p. 108802, 2016; https://doi.org/10.1088/1674-1056/25/10/108802

[34] L. Ma, F. Hao, C. C. Stoumpos, B. T. Phelan, M. R. Wasielewski, and M. G. Kanatzidis, "Carrier Diffusion Lengths of over 500 nm in Lead-Free Perovskite CH3NH3SnI3 Films," Journal of the American Chemical Society, vol. 138, no. 44, pp. 14750-14755, 2016/11/09 2016; https://doi.org/10.1021/jacs.6b09257

[35] Z. Zhao, F. Gu, Y. Li, W. Sun, S. Ye, H. Rao, Z. Liu, Z. Bian, and C. Huang, "Mixed-Organic-Cation Tin Iodide for Lead-Free Perovskite Solar Cells with an Efficiency of 8.12%," Advanced Science, vol. 4, no. 11, p. 1700204, 2017; https://doi.org/10.1002/advs.201700204

[36] F. Hao, C. C. Stoumpos, D. H. Cao, R. P. H. Chang, and M. G. Kanatzidis, "Lead-free solid-state organic-inorganic halide perovskite solar cells," Nature Photonics, vol. 8, no. 6, pp. 489-494, 2014/06/01 2014; https://doi.org/10.1038/nphoton.2014.82

[37] Y. Takahashi, H. Hasegawa, Y. Takahashi, and T. Inabe, "Hall mobility in tin iodide perovskite CH3NH3SnI3: Evidence for a doped semiconductor," Journal of Solid State Chemistry, vol. 205, pp. 39-43, 2013/09/01/ 2013; https://doi.org/10.1016/j.jssc.2013.07.008

[38] S. Mishra, K. Bhargava, and D. Deb, "Numerical simulation of potential induced degradation

(PID) in different thin-film solar cells using SCAPS-1D," Solar Energy, vol. 188, pp. 353-360, 2019/08/01/ 2019; https://doi.org/10.1016/j.solener.2019.05.077

[39] Y. M. Lee, I. Maeng, J. Park, M. Song, J.-H. Yun, M.-C. Jung, and M. Nakamura, "Comprehensive understanding and controlling the defect structures: An effective approach for organic-inorganic hybrid perovskite-based solar-cell application," Frontiers in Energy Research, vol. 6, p. 128, 2018; https://doi.org/10.3389/fenrg.2018.00128

[40] F. Hao, C. C. Stoumpos, P. Guo, N. Zhou, T. J. Marks, R. P. H. Chang, and M. G. Kanatzidis, "Solvent-Mediated Crystallization of CH3NH3SnI3 Films for Heterojunction Depleted Perovskite Solar Cells," Journal of the American Chemical Society, vol. 137, no. 35, pp. 11445-11452, 2015/09/09 2015; https://doi.org/10.1021/jacs.5b06658

[41] T. Minemoto and M. Murata, "Device modeling of perovskite solar cells based on structural similarity with thin film inorganic semiconductor solar cells," Journal of applied physics, vol. 116, no. 5, p. 054505, 2014; https://doi.org/10.1063/1.4891982

[42] C. C. Stoumpos, C. D. Malliakas, and M. G. Kanatzidis, "Semiconducting Tin and Lead Iodide Perovskites with Organic Cations: Phase Transitions, High Mobilities, and Near-Infrared Photoluminescent Properties," Inorganic Chemistry, vol. 52, no. 15, pp. 9019-9038, 2013/08/05 2013; https://doi.org/10.1021/ic401215x

[43] F. Behrouznejad, S. Shahbazi, N. Taghavinia, H.-P. Wu, and E. Wei-Guang Diau, "A study on utilizing different metals as the back contact of CH3NH3PbI3 perovskite solar cells," Journal of Materials Chemistry A, 10.1039/C6TA05938D vol. 4, no. 35, pp. 13488-13498, 2016; https://doi.org/10.1039/C6TA05938D

[44] S. Rai, B. K. Pandey, and D. K. Dwivedi, "Modeling of highly efficient and low cost CH3NH3Pb(I1-xClx)3 based perovskite solar cell by numerical simulation," Optical Materials, vol. 100, p. 109631, 2020/02/01/ 2020; https://doi.org/10.1016/j.optmat.2019.109631

[45] F. Anwar, R. Mahbub, S. S. Satter, and S. M. Ullah, "Effect of Different HTM Layers and Electrical Parameters on ZnO Nanorod-Based Lead-Free Perovskite Solar Cell for High-Efficiency Performance," International Journal of Photoenergy, vol. 2017, p. 9846310, 2017; https://doi.org/10.1155/2017/9846310

[46] Y. Gan, X. Bi, Y. Liu, B. Qin, Q. Li, Q. Jiang, and P. Mo, "Numerical investigation energy conversion performance of tin-based perovskite solar cells using cell capacitance simulator," Energies, vol. 13, no. 22, p. 5907, 2020; https://doi.org/10.3390/en13225907

[47] I. Alam and M. A. Ashraf, "Effect of different device parameters on tin-based perovskite solar cell coupled with In2S3 electron transport layer and CuSCN and Spiro-OMeTAD alternative hole transport layers for high-efficiency performance," Energy Sources, Part A: Recovery, Utilization, and Environmental Effects, pp. 1-17, 2020; https://doi.org/10.1080/15567036.2020.1820628

[48] P. Roy, N. Kumar Sinha, and A. Khare, "An investigation on the impact of temperature variation over the performance of tin-based perovskite solar cell: A numerical simulation approach," Materials Today: Proceedings, vol. 39, pp. 2022-2026, 2021/01/01/ 2021; https://doi.org/10.1016/j.matpr.2020.09.281